Parity-violating asymmetry in quasielastic *e-d* scattering

E. Hadjimichael
Department of Physics, Fairfield University, Fairfield, Connecticut 06430

G. I. Poulis and T. W. Donnelly
Center for Theoretical Physics, Laboratory for Nuclear Science, and Department of Physics, Massachusetts Institute of Technology, Cambridge, Massachusetts 02139

(Received 14 January 1992)

Results are presented for (inclusive) parity-violating quasielastic electron scattering of polarized electrons from deuterium. The sensitivity of the asymmetry to interference effects, to the presence or absence of final-state interactions, to the choice of *NN* interaction, and to specifics of nucleon form factors is investigated within the framework of the standard model for the electroweak interaction. The calculations span a range of momentum transfers from low values, where a nonrelativistic treatment including a realistic *NN* interaction is appropriate, to beyond 1 GeV/*c*, where a relativistic plane-wave impulse approximation is employed. We find favorable kinematical regions for experiments at medium-energy (MIT–Bates, Mainz) and higher-energy (CEBAF) electron accelerators where issues relating to the nucleon's axial-vector and strangeness form factors can be addressed.

PACS number(s): 24.80.Dc, 25.10.+s, 25.30.Bf

I. INTRODUCTION

In this work we take as given the standard model [1] of the electroweak interaction at tree level, and focus our attention on the roles played by nucleon structure and *NN* dynamics in the determination of the parity-violating (PV) asymmetry in polarized quasielastic (QE) electron scattering from deuterium. We study the parity-violating helicity asymmetry resulting from the interference between the electromagnetic one-photon exchange process in Fig. 1(a) and the weak one-boson exchange process in Fig. 1(b). We shall not repeat much of the basic formalism required in PV studies [2–7], since this has been presented at length in previous work. In particular, many of the features developed here specifically for the deuteron have recently been explored in a more general context for PV QE scattering from nuclei using the Fermi gas model [8]. In focusing on the processes shown in Fig. 1, contributions to the asymmetry due to the effects of PV *NN* interactions in the initial (bound ^{2}H) and final (continuum *np*) states themselves are neglected. Previous studies [9] of admixing odd-parity states into the deuteron ground state via such interactions have shown these *PV* effects to be small for the case of photodisintegration, suggesting that neglecting them should be a good approximation for electrodisintegration near the QE peak. However, further work in this kinematic region should be undertaken in order to confirm that the effects are indeed negligible.

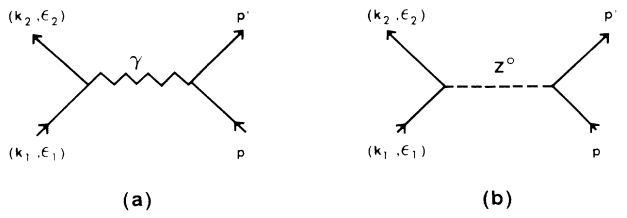

FIG. 1. The elementary electron-nucleon interaction processes occurring via (a) photon exchange (electromagnetic current) and (b) Z^0 exchange (weak neutral current).

Our ultimate objectives will be to map out the parity-violating asymmetry in polarized *e-d* scattering over a fairly wide kinematical range from about 10 MeV/*c* to 1–2 GeV/*c* in momentum transfer *q* and from electrodisintegration threshold up to where pion production becomes important, and to study the interplay of the dynamics of the $A=2$ system with the single-nucleon form factor content. Of special interest here are the roles played by the nucleon's axial-vector and strangeness form factors. The main focus of the present work is on the QE peak where the electroweak excitation process is presumed to be well represented as "quasifree," although some results are also given for kinematics away from the peak. In future work we shall return to detail the nature of the PV asymmetry in "non-quasi-free" kinematics.

Since we must have extremely high confidence in our ability to model the nuclear physics aspects of the problem if we are to have any hope of shedding light on the nature of the single-nucleon form factors (for instance, on the strangeness content of the nucleon), one of our concerns is to examine the validity of the various approximations which are at some level inevitable, even when dealing with a system as simple as the deuteron. For momentum transfer of less than a few hundred MeV/*c*, we expect to rely for theoretical predictions on a model in which the *np* system is described by nonrelativistic wave functions for the initial (bound) and final (scattering)

states, namely, as solutions of the Schrödinger equation. Such an approach incorporates the effects of final-state interactions (FSI) including orthogonality. One of our goals here is to examine the sensitivity of the PV asymmetry to the choice of *NN* interaction.

To delve somewhat further into how the nature of the final state enters into the inclusive cross section and PV asymmetry, we also present results in which the FSI have been "turned off." In particular, the plane-wave Born approximation (PWBA) [10] is obtained from the FSI model by replacing the final interacting *np* state by a plane-wave state. In addition to lacking FSI, this model suffers from lack of orthogonality in the $^3S_1+{}^3D_1$ channel between the initial and final states, a defect which is expected to be more pronounced at lower energies where the lower partial waves in the final state are dominant. The amplitudes which enter into the coincidence reactions, $^2\mathrm{H}(e,e'p)n$ or $^2\mathrm{H}(e,e'n)p$, are shown schematically in Fig. 2. For the former the photon (or Z^0) may interact with a proton that is then detected, as indicated in Fig. 2(a); alternatively, the photon may interact with a neutron and the other particle in the final state (the proton) is then detected, as indicated in Fig. 2(b). For the $^2\mathrm{H}(e,e'n)p$ reaction protons and neutrons are interchanged in the two parts of the figure. The cross sections are obtained by squaring the sum of all amplitudes that have the same experimentally fixed conditions, in particular, an outgoing proton (neutron) with a specific momentum for $^2\mathrm{H}(e,e'p)n$ [$^2\mathrm{H}(e,e'n)p$]. As long as the final-state conditions are the same, the two diagrams can interfere; thus the cross section involves terms which arise from the squares of all allowed amplitudes (we call these 'direct" contributions, $\mathcal{D}$) and terms which arise from all interferences between amplitudes where the photon or Z^0 connects to a proton and where it connects to a neutron (called "exchange" contributions, $\mathcal{E}$). Finally, to obtain the inclusive cross section we perform the sum/integral over all kinematically allowed final states. Even at the level of inclusive scattering there remain both $\mathcal{D}$ and $\mathcal{E}$ contributions to the cross section and PV asymmetry. Of course, terms of both types are automatically included in the FSI model. The merit of the PWBA is that it will allow us to see how much the asymmetry is sensitive to the interference contributions (which are frequently neglected in other treatments such as the PWIA discussed below, especially for nuclei having $A>2$) and how much it is sensitive to orthogonality and the additional distortion effects of the FSI. Both the model with FSI and the usual PWBA, however, involve nonrelativistic expansions of the electroweak currents to order $(q/M)^2$, where M is the nucleon mass, and so become suspect when results at high q are required.

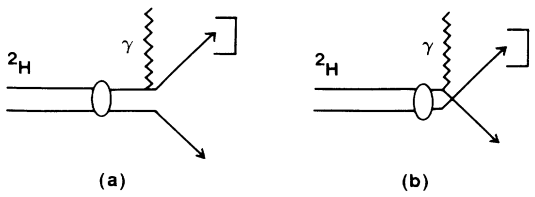

FIG. 2. Electrodisintegration of the deuteron in the absence of final-state interactions (FSI). In PWIA, processes (a) and (b) having the proton as the struck nucleon contribute incoherently with equivalent ones where the neutron is the struck nucleon, yielding the direct term $\mathcal{D}$. In PWBA, the two sets of processes contribute coherently (i.e., an *np* interference contribution, the exchange term $\mathcal{E}$, is included).

In extending our discussions of PV electron scattering to high-momentum transfer, we are led to consider a more covariant approach, that of the factorized relativistic plane-wave impulse approximation (PWIA) [10–12], which has often been employed in interpreting parity-conserving (PC) quasielastic data in similar situations when relativistic effects become important. Here the cross section is factored into two terms, (1) the spectral function which represents the probability that a nucleon in the deuteron will be found with a given momentum and energy, and (2) the half-off-shell single-nucleon cross section. A model that is frequently invoked for the latter involves the parametrization cc1 of de Forest [12]; in the present work, we present an extension of that model to incorporate weak neutral currents, including axial-vector as well as vector contributions. Since the fully relativistic electroweak single-nucleon cross sections are employed [i.e., without requiring expansions in $(q/M)^n$], there is some hope that the PV asymmetry can be modeled successfully at rather large values of momentum transfer q and energy transfer ω. Of course, the PWIA has its own limitations, the primary ones being that FSI and the interference effects are both neglected (i.e., in the latter case, the $\mathcal{D}$ contributions are retained whereas the $\mathcal{E}$ terms are set to zero). One of our aims in the present work is to show that the interference effects (as contained in the PWBA) or effects of FSI (which occur when realistic *NN* potentials are employed) are negligible under certain circumstances at high q and ω, so that the PWIA may be valid. Accordingly, we will conclude that, at least within the context of the models we employ, it is possible to control the nuclear model uncertainties in the PV asymmetry at the 1–2 % level by using the approach best suited to the kinematics of interest—nonrelativistic models with FSI at low-to-medium values of q and the relativistic PWIA model at high q.

Our final objective in this work is to determine how the asymmetry depends on the various vector and axial-vector form factors of the nucleon, including the possibility of form factors which arise from nonzero strange-quark-antiquark ($\bar{s}s$) configurations in the nucleon. We shall see that the deuteron appears to provide a rather special testing ground for such form factor studies, since our results suggest that nuclear model uncertainties in QE scattering are small enough to permit the interpretation of the PV asymmetry to be undertaken at the few % level. For comparison, while there is also reason to be optimistic in the cases of heavier nuclei, the simplicity and calculability of the $A=2$ system make it particularly well suited to such investigations. What emerges from our work is motivation for undertaking experimental studies both of the deuteron and of the nucleon itself: the two cases have rather different dependences on some of

the nucleon form factors and, consequently, these dependences can be separated in such complementary work, whereas they could not be extracted in one case alone.

We summarize the essential features of the formalism employed in this work in Sec. II, beginning with a review of the basic observables needed in treating PV electron scattering (Sec. II A). This is followed by a brief section (II B) where the various single-nucleon form factors are introduced. In Sec. II C we discuss the models employed for PV (and PC) inclusive QE electron scattering. We begin in Sec. II C 1 with the simplest model, *viz.*, the "static" approximation where the nucleus is represented as an incoherent set of noninteracting nucleons at rest. This provides a starting point in estimating the size of the asymmetry and so the feasibility of potential measurements in the QE region. We then proceed to discuss three more sophisticated nuclear models for deuteron electrodisintegration: the nonrelativistic model with FSI (Sec. II C 2), the factorized relativistic PWIA (Sec. II C 3), and the PWBA (Sec. II C 4). Our results are presented in Sec. III, beginning in Sec. III A with a discussion of the nuclear model dependences that emerge. Here the basic models listed above are used to predict the PV asymmetry as reliably as we can at present and, additionally, to gain insight into what effects (*NN* interaction, $\mathscr{E}/\mathscr{D}$ interference, orthogonality, relativity) play the dominant roles in specifying the remaining nuclear physics uncertainties in the asymmetry. Finally, we end the present discussions in Sec. IV with a few concluding remarks.

II. FORMALISM

A. Basic parity-violating electron scattering formalism

Let us begin with a brief summary of the forms taken by the electromagnetic (EM) cross section and PV asymmetry for inclusive quasielastic electron scattering. In particular, for later use, we shall need to display the way that the five basic nuclear response functions enter into these quantities. The kinematics for electron scattering with a single photon or Z^0 exchange are shown in Figs. 1(a) and 1(b). Here an electron with momentum $\mathbf{k}_1$ and energy ϵ_1 scatters to a final state with $\mathbf{k}_2$ and ϵ_2. We shall invoke the extreme relativistic limit ($|\mathbf{k}_1| \approx \epsilon_1 \gg m_e, |\mathbf{k}_2| \approx \epsilon_2 \gg m_e$, where m_e is the electron mass), since generally the electron energies will range from hundreds of MeV to several GeV. The magnitude of the four-momentum transfer is then given by

$$|Q^2| = q^2 - \omega^2 = 4\epsilon_1\epsilon_2 \sin^2\frac{\theta}{2} , \tag{1}$$

where $q = |\mathbf{q}|$ and ω are the three-momentum and energy transfer, and θ is the electron scattering angle. In the laboratory frame, the electromagnetic—parity conserving—cross section for inclusive scattering of unpolarized electrons has the general form [13,14]

$$\frac{d^2\sigma}{d\Omega\, d\epsilon_2} = \sigma_M [v_L R^L(q,\omega) + v_T R^T(q,\omega)] = \sigma_M W^{\rm EM} , \tag{2}$$

where L and T refer to the deuteron response functions for the longitudinal and transverse projections of the nuclear electromagnetic current with respect to $\mathbf{q}$, and σ_M is the Mott cross section

$$\sigma_M = \left[\frac{\alpha \cos(\theta/2)}{2\epsilon_2 \sin^2(\theta/2)} \right]^2 , \tag{3}$$

with α the fine-structure constant. The lepton kinematics are included in the factors

$$v_L = \left[\frac{Q^2}{q^2} \right]^2 , \quad v_T = \frac{1}{2} \left| \frac{Q^2}{q^2} \right| + \tan^2\frac{\theta}{2} . \tag{4}$$

The PV asymmetry can be cast in a form similar to these electromagnetic results. On the one hand, the cross section in Eq. (2), for unpolarized electron scattering, is the average of two cross sections for polarized electrons with helicity $h = \pm 1$:

$$\left[\frac{d^2\sigma}{d\Omega\, d\epsilon_2} \right]^{\rm EM} = \frac{1}{2} \left[\frac{d^2\sigma^+}{d\Omega\, d\epsilon_2} + \frac{d^2\sigma^-}{d\Omega\, d\epsilon_2} \right] . \tag{5}$$

On the other hand, the difference between the two cross sections is a measure of parity violation [2–8] which arises from interference between the processes in Figs. 1(a) and 1(b):

$$\left[\frac{d^2\sigma}{d\Omega\, d\epsilon_2} \right]^{\rm PV} = \frac{1}{2} \left[\frac{d^2\sigma^+}{d\Omega\, d\epsilon_2} - \frac{d^2\sigma^-}{d\Omega\, d\epsilon_2} \right] = \mathcal{A}_0 \sigma_M W^{\rm PV} , \tag{6}$$

where the coefficient $\mathcal{A}_0$ is

$$\mathcal{A}_0 \equiv \frac{G|Q|^2}{2\sqrt{2}\pi\alpha} \tag{7}$$

and G is the Fermi constant. In terms of parity-violating response functions R^L_{AV}, $R^{T'}_{AV}$, and $R^{T'}_{VA}$, the quantity $W^{\rm PV}$ is given by

$$W^{\rm PV} = v_L R^L_{AV} + v_T R^T_{AV} + v_{T'} R^{T'}_{VA} , \tag{8}$$

where the extra lepton kinematical factor is given by

$$v_{T'} = \tan\frac{\theta}{2} \left[\left| \frac{Q^2}{q^2} \right| + \tan^2\frac{\theta}{2} \right]^{1/2} . \tag{9}$$

The subscript AV (and VA) in the PV response functions indicates the interference of leptonic axial $\times$ hadronic vector currents (and the reverse). Finally, the parity-violating asymmetry $\mathcal{A}$ is defined by

$$\mathcal{A} = \left[\frac{d^2\sigma}{d\Omega\, d\epsilon_2} \right]^{\rm PV} \Big/ \left[\frac{d^2\sigma}{d\Omega\, d\epsilon_2} \right]^{\rm EM} = \frac{d^2\sigma^+ - d^2\sigma^-}{d^2\sigma^+ + d^2\sigma^-} \equiv \mathcal{A}_0 \frac{W^{\rm PV}}{W^{\rm EM}} . \tag{10}$$

The response functions in the above equations arise from contractions of the matrix elements of the leptonic

and hadronic currents. The EM (vector) leptonic current is given by the familiar form,

$$j_\mu^{\rm EM}=i\bar{u}_{s'}(k_2)\gamma_\mu u_s(k_1)\ , \tag{11}$$

where s and s' label the electron helicities. Analogously, as discussed in detail in Refs. [2,3], the leptonic weak neutral current (WNC) matrix elements are composed of a vector (V) and an axial-vector (A) part

$$j_\mu^{\rm WNC}=i\bar{u}_{s'}(k_2)[a_V\gamma_\mu+a_A\gamma_5\gamma_\mu]u_s(k_1)\ . \tag{12}$$

In the standard model [1–3], the leptonic couplings are given by

$$\begin{aligned} a_V&=-(1-4\sin^2\theta_W)\cong-0.092\ ,\\ a_A&=-1\ , \end{aligned} \tag{13}$$

where we adopt the value $\sin^2\theta_W=0.227$ in the present work [15–17]. General hadronic (nuclear) current matrix elements, $(J_{fi}^{\rm EM})_\mu$ and $(J_{fi}^{\rm WNC})_\mu$, must then be contracted with their leptonic counterparts to yield cross sections and asymmetries involving contractions of leptonic with hadronic tensors $\eta_{\mu\nu}$ and $W^{\mu\nu}$, respectively. The steps leading to such expressions, where results are written in terms of the five different response functions entering in inclusive PC and PV electron scattering, are given in detail in Refs. [2–8].

B. Single-nucleon form factors

Since one of our prime motivations in the present work is to study the hadronic structure of the nucleon itself as a constituent in the two-body system, in this section we list the various form factors which enter in PV electron scattering. The single-nucleon current matrix elements of the electromagnetic and weak neutral currents can be expressed in the following forms:

$$J_\mu^{\rm EM}=i\bar{u}_{\Lambda'}(p')\left[F_1\gamma_\mu+\frac{i}{2M}F_2\sigma_{\mu\nu}q^\nu\right]u_\Lambda(p)\ , \tag{14}$$

where Λ (Λ') label the nucleon spins, $p'_\mu-p_\mu=q_\mu$ is the four-momentum transfer, and where p_μ,p'_μ are defined in Fig. 1 to be the initial and final nucleon momenta, respectively. $F_{1,2}$ are the Dirac and Pauli form factors of the nucleon (different for proton and neutron) and they are functions of the four-momentum transfer $Q^2=q_\mu q^\mu$. They can be re-expressed in terms of Sachs [18] form factors ($G_{E,M}$) in the usual way; in the present work we choose to use the Sachs form factors throughout. The weak neutral current for the single nucleon has a similar structure. First, it has both vector and axial-vector contributions:

$$J_\mu^{\rm WNC}=\tilde{J}_\mu^{\,V}+\tilde{J}_\mu^{\,A}\ , \tag{15}$$

where the tilde indicates that this is the weak neutral current. The vector $\tilde{J}_\mu^{\,V}$ has the same form as the (vector) EM current given in Eq. (14), but with form factors (F's, or the corresponding G's) now indicated with tildes (see below). Of course, there is also an axial-vector current to be considered:

$$\tilde{J}_\mu^{\,A}=i\bar{u}_\Lambda(p')(\tilde{G}_A\gamma_\mu\gamma_5)u_\Lambda(p)\ , \tag{16}$$

where $\tilde{G}_A$ is the weak neutral current axial form factor of the nucleon (proton or neutron). The WNC form factors of the proton and neutron can be written in the following way [6–8]:

$$\begin{aligned} \tilde{G}_{Ep,En}&=(\beta_V^pG_{Ep,En}+\beta_V^nG_{En,Ep})-\tfrac{1}{2}G_E^{(s)}\ ,\\ \tilde{G}_{Mp,Mn}&=(\beta_V^pG_{Mp,Mn}+\beta_V^nG_{Mn,Mp})-\tfrac{1}{2}G_M^{(s)}\ ,\\ \tilde{G}_{Ap,An}&=(\beta_A^pG_{Ap,An}+\beta_A^nG_{An,Ap})-\tfrac{1}{2}G_A^{(s)}\ , \end{aligned} \tag{17}$$

where the hadronic weak neutral current couplings are given in the standard model at tree level by [2–8]

$$\begin{aligned} \beta_V^p&=\tfrac{1}{2}(1-4\sin^2\theta_W)\cong0.046\ ,\\ \beta_V^n&=-\tfrac{1}{2}\ ,\\ \beta_A^p&=-\beta_A^n=\tfrac{1}{2}\ . \end{aligned} \tag{18}$$

The form factors here include the familiar electromagnetic ones, $G_{Ep,En}$ and $G_{Mp,Mn}$; the axial-vector cases, $G_A^{(1)}=G_{Ap}-G_{An}$, which also occurs in beta decay, together with its isoscalar partner $G_A^{(0)}=G_{Ap}+G_{An}$, which does not enter in the present situation due to the last identity in Eqs. (18); and form factors, $G_{E,M,A}^{(s)}$, which enter when the nucleon has nonzero $\bar{s}s$ strangeness components. In the discussions to follow it will prove useful to have all of the form factors expressed in terms of isoscalar ($T=0$) and isovector ($T=1$) contributions, $\mathcal{G}_X^{(0)}=\mathcal{G}_{X_p}+\mathcal{G}_{X_n}$ and $\mathcal{G}_X^{(1)}=\mathcal{G}_{X_p}-\mathcal{G}_{X_n}$, where $\mathcal{G}=G$ or $\tilde{G}$ and $X=E,M$ or A. Note that all of the strangeness content is isoscalar. In Refs. [6–8] convenient parametrizations are given for the form factors, which we have employed in the present work as well. We shall also need the isoscalar and isovector weak neutral current hadronic couplings [similar combinations of the proton and neutron couplings in Eqs. (18)]: $\beta_V^{(0)}=-2\sin^2\theta_W\cong-0.454$, $\beta_V^{(1)}=1-2\sin^2\theta_W\cong0.546$, $\beta_A^{(0)}=0$, and $\beta_A^{(1)}=1$.

C. Models of the ^{2}He$(\vec{e},e')np$ reaction

As discussed in the Introduction, a main concern in this work is in the range of validity of the various approximations that must be made in describing the interacting np system and in treating the electroweak interaction with it. The reliability of these approximations in different kinematical regions is reflected in our ability to extract information about single-nucleon form factors in studies of the asymmetry in PV electron scattering from deuterium. Here we have employed four different models: (1) the static approximation, which is used as a simple guide to the nature of the PV asymmetry; (2) the nonrelativistic model with final state interactions, which incorporates aspects of the nuclear dynamics that are essential at low-momentum transfer (where FSI effects are important); (3) the plane-wave impulse approximation, which allows us to address some of the questions involving relativistic effects at high q; and (4) the plane-

wave Born approximation, which serves as a bridge between the previous two models. Models (1) and (4) are presented for the purpose of gaining an appreciation for the refinements incorporated in the other two models; the latter are the ones used in presenting our final results, specifically (see Sec. III), model (2) for momentum transfers below some characteristic value and model (3) for high q.

$$\frac{\mathcal{A}}{\mathcal{A}_0}=\left\{a_A\left[v_L[(q^2/2|Q^2|)(ZG_{E_p}\tilde{G}_{E_p}+NG_{En}\tilde{G}_{En})]+v_T[\tau(ZG_{Mp}\tilde{G}_{Mp}+NG_{Mn}\tilde{G}_{Mn})]\right]\right.$$
$$\left.+a_V\left[v_{T'}[\sqrt{\tau(1+\tau)}(ZG_{Mp}\tilde{G}_{Ap}+NG_{Mn}\tilde{G}_{An})]\right]\right\}\left[v_L[(q^2/2|Q^2|)(ZG_{Ep}^2+NG_{En}^2)]+v_T[\tau(ZG_{Mp}^2+NG_{Mn}^2)]\right]^{-1} \tag{19}$$

where Z and N are the proton and neutron numbers of a general nucleus, respectively, and where $\tau=|Q^2|/4M^2$ is the dimensionless four-momentum transfer. Note that elastic scattering from the proton can be recovered simply by setting $Z=1$ and $N=0$. The static approximation can be derived using as a starting point either the Fermi gas model [8] or the PWIA [10–12] (see also Sec. II C 3). It provides a simple expression which can be used in estimating the feasibility of PV experiments in the QE region. As we shall see in Sec. III, it is quite successful when applied at the QE peak, but not when other kinematics are required.

2. Nonrelativistic calculations with final-state interactions (FSI)

We now proceed to more sophisticated models than the static approximation discussed briefly above. In our treatment of the *np* system in terms of nonrelativistic solutions of the Schrödinger equation with realistic *NN* potentials, we follow the usual approach and expand the single-nucleon current matrix elements above in powers of $(1/M)$. Specifically, in the transverse projections of the current we take only the lowest nontrivial order, whereas in the charge projections of the vector current we include terms of order $(q/M)^2$ (Darwin-Foldy and spin-orbit terms [13]). Converting from momentum space to coordinate space, we obtain the familiar operators generally used in electromagnetic studies, together with their neutral current extensions, and the lowest-order forms of the axial-vector currents (the neutral current analogs of those used in discussions of charge-changing weak interaction processes such as beta decay). The same strategy is employed in the PWBA treatment which differs from the full FSI calculations in that plane waves are used for the *np* final state (see also Sec. II C 4).

Let us begin with the electromagnetic case. There the inclusive cross section, differential in the outgoing electron energy and scattering angle, is given by

$$\frac{d^2\sigma}{d\epsilon_2\,d\Omega_2}=\frac{2\alpha^2}{(2\pi)^3}\frac{\epsilon_2}{\epsilon_1}\int d^3p\frac{\delta(E_f-M_D+\omega)}{Q^4}\sum_{i,f}\eta_{\mu\nu}W^{\mu\nu}\,, \tag{20}$$

where the integration is over the momentum of the outgoing nucleon. The invariant product of the leptonic and hadronic tensors, $\eta_{\mu\nu}W^{\mu\nu}$, can be evaluated in either the laboratory or the center-of-mass frame of the *np* system. We choose the latter and find

$$\begin{aligned}\frac{d^2\sigma}{d\epsilon_2\,d\Omega_2}&=\frac{\sigma_M}{(2\pi)^2}\frac{\hat{p}_p\hat{E}_n}{\gamma(\hat{E}_p+\hat{E}_n)}\\&\quad\times\int_{-1}^{1}d\chi E_p(\chi)(v_L\xi^2\hat{W}^L+v_T\hat{W}^T)\\&=\sigma_M(v_LR^L+v_TR^T)\\&=\sigma_M W^{\rm em}\,,\end{aligned} \tag{21}$$

where $\xi=q^2/\hat{q}^2$ results from the Lorentz transformation from c.m. to laboratory coordinates. The subscripts p and n refer to the proton and the neutron, and quantities marked with a caret are to be evaluated in the c.m. frame of the *np* system. The c.m. nucleon momenta $\hat{p}_p=-\hat{p}_n$ and energies $\hat{E}_{p,n}$ are uniquely determined by the electron scattering variables (q,ω) in the laboratory system. The laboratory nucleon momenta and energies may then be expressed in terms of the c.m. quantities; for example, one finds that $E_p(\chi)=\gamma(\hat{E}_p+\beta\hat{p}_p\chi)$, where $\beta=q/(M_D+\omega)$ and $\gamma=1/\sqrt{1-\beta^2}$ arise from the Lorentz transformation between c.m. and laboratory systems, and where $\chi=\cos\hat{\theta}_p$, with $\hat{\theta}_p$ being the angle between the outgoing proton and the three-momentum transfer in the c.m. system. The structure functions R^L and R^T are proportional to the integrals defined in Eq. (21), which can be shown to be given by

1. The static approximation

The present study of PV in the reaction $^2\mathrm{H}(\vec{e},e')np$ is focused on the kinematic region around the quasielastic peak where, in the "static" approximation (which is the simplest of the models used in the present work) the nuclear matrix elements involve incoherent sums of matrix elements of the single-nucleon at rest [4,6–8]:

$$\int_{-1}^{1} d\chi E_p(\chi)\hat{W}^L = \frac{(4\pi)^2}{3\hat{k}^2} 2\gamma \hat{E}_p \sum_{J_f,J} \left[\sum_L |Y^t_{J_f,J,L}|^2 + |Y^s_{J_f,J}|^2 \right] ,$$
$$\int_{-1}^{1} d\chi E_p(\chi)\hat{W}^T = \frac{(4\pi)^2}{3\hat{k}^2} 2\gamma \hat{E}_p \frac{1}{2M^2} \sum_{\lambda=1,2} \sum_{J_f,J} \left[\sum_L |X^t_{J_f,J,L,\lambda}|^2 + |X^s_{J_f,J,\lambda}|^2 \right] . \tag{22}$$

Here $\hat{k}$ is the relative np momentum in the c.m. frame and the quantities $Y^{t,s}$ and $X^{t,s}$ are reduced matrix elements of the nuclear charge density and nuclear current, respectively, taken between the deuteron ground state and the np triplet (t) and singlet (s) final state expanded in partial waves. The EM operators are those obtained as discussed above. In the present calculation we have included partial waves up to $J_f=17$, with J and L assuming the values J_f-1, J_f, J_f+1, where J is the rank of the electromagnetic operator and L is the orbital angular momentum in the final state. In the model with FSI, the first seven of these partial waves are solutions of the Schrödinger equation with the NN interaction, and the rest are plane-wave solutions. In the PWBA the calculation is just as outlined here, except that all partial waves are plane-wave solutions (see also the discussions to follow in Sec. II C 4).

Turning now to the parity-violating response functions, the numerator of the PV asymmetry which involves $W^{\rm PV}$ [see Eqs. (8) and (10)] is calculated using the same procedures as those discussed above for the electromagnetic case. In particular, R^L_{AV}, R^T_{AV}, and $R^{T'}_{VA}$ are obtained in the same way as the electromagnetic response functions R^L and R^T by replacing $|Y|^2$ and $|X|^2$ in Eqs. (22) with the following: R^L_{AV} is obtained from R^L by the replacement

$$\sum_L |Y^t_{J_f,J,L}|^2 + |Y^s_{J_f,J}|^2 \to a_A \left[\sum_L Y^{t\,*}_{J_f,J,L} \bar{Y}^{\,t}_{J_f,J,L} + Y^{s\,*}_{J_f,J} \bar{Y}^{\,s}_{J_f,J} \right] , \tag{23a}$$

R^T_{AV} from R^T by the replacement

$$\sum_L |X^t_{J_f,J,L,\lambda}|^2 + |X^s_{J_f,J,\lambda}|^2 \to a_A \left[\sum_L X^{t\,*}_{J_f,J,L,\lambda} \bar{X}^{\,t}_{J_f,J,L,\lambda} + X^{s\,*}_{J_f,J,\lambda} \bar{X}^{\,s}_{J_f,J,\lambda} \right] , \tag{23b}$$

and $R^{T'}_{VA}$ from R^T by the replacement

$$\sum_L |X^t_{J_f,J,L,\lambda}|^2 + |X^s_{J_f,J,\lambda}|^2 \to a_V \left[\sum_L X^{t\,*}_{J_f,J,L,\lambda} \bar{\bar{X}}^{\,t}_{J_f,J,L,\lambda} + X^{s\,*}_{J_f,J,\lambda} \bar{\bar{X}}^{\,s}_{J_f,J,\lambda} \right] . \tag{23c}$$

The quantities $\bar{X}^{t,s}$, $\bar{Y}^{t,s}$ are obtained in the same way as $X^{t,s}$, $Y^{t,s}$, except now using the (vector) weak neutral current form factors $\tilde{G}_{E,M}$, instead of the electromagnetic ones $G_{E,M}$, as required in Eqs. (22). The quantities $\bar{\bar{X}}^{t,s}$ involve the axial-vector current matrix elements introduced above. By comparing the nonrelativistic limits of the matrix elements of $i\sigma_{\mu\nu}q^\nu/2M$ [see Eq. (14)] with those of $\gamma_\mu\gamma_5$ [see Eq. (16)], it is straightforward to see that these quantities are obtained from $X^{t,s}$ by retaining only the parts which contain the Pauli form factors F_{2p} and F_{2n} in Eqs. (22) and replacing $(q/2M)F_{2p,n}$ by $\tilde{G}_{Ap,n}$ to account for the different single-nucleon form factors and factor $q/2M$ which occur in the two cases. This simple relationship between the spin matrix elements (vector and axial vector) only pertains in the leading nonrelativistic limit. Note also for future reference that the strangeness content has now been built into the matrix elements $\bar{Y}^{t,s}$, $\bar{X}^{t,s}$, and $\bar{\bar{X}}^{t,s}$, through the use of the weak neutral current form factors $\tilde{G}_{E,M,A}$ given in Eqs. (17).

3. *Factorized relativistic plane-wave impulse approximation (PWIA)*

For the PWIA approach [10–12] a different procedure is followed: since the problem factorizes by construction, we need single-nucleon cross sections and must multiply these by the probability that the struck nucleon has specified values of energy and momentum, *viz.*, by the nuclear spectral function. The spectral function required in studying the reaction ^{2}H$(\vec{e},e')np$ simply involves the deuteron momentum distribution $\rho(p)$. Inclusive electron scattering is then obtained by performing the average-over-initial and sum-over-final states (see Ref. [19] for details). Following the usual practice in electromagnetic studies, we use some prescription for the half-shell single-nucleon cross section such as $\sigma^{\rm EM}_{\rm cc1}$, the cc1 form of de Forest [12]. In the present work we shall also employ this form together with a generalization, $\sigma^{\rm PV}_{\rm cc1}$, for use in the relativistic PWIA description of PV electron scattering. We have investigated the on-shell limit of cc1 and found the off-shell effects to be negligible. It may prove interesting to explore other off-shell parametrizations, although our expectation is that the effects are much less important than the ones addressed in the present work.

The PWIA has at least two characteristic aspects: it involves the use of plane-wave final states and, moreover, takes into account only the incoherent sum over the squares of the amplitudes of the process depicted in Figs. 2(a) and 2(b) for the case of the deuteron. This provides what was called the direct ($\mathcal{D}$) contribution above, to be contrasted with the exchange ($\mathcal{E}$) term which arises from the interference between the two amplitudes. The latter is ignored in the PWIA, but is included in the PWBA (see below) or in the full results with FSI discussed above. The PWIA inclusive response functions that enter in Eqs. (2) and (8) can be shown to have the following forms [19]:

$$R^K(T=0,1)=\frac{\pi M^2}{q}\int_{|y|}^{Y} dp\, p\rho(p)\frac{1}{\bar{E}}W^K(T=0,1)\ , \tag{24a}$$

$$\tilde{R}^K(T=0,1)=\frac{\pi M^2}{q}\int_{|y|}^{Y} dp\, p\rho(p)\frac{1}{\bar{E}}\tilde{W}^K(T=0,1)\ , \tag{24b}$$

where the limits of integration are specific functions of q and ω; at reasonably high q and small $|y|$ the upper limit can be extended to infinity, $Y\to\infty$ (see Refs. [19,20]). The responses are labeled by isospin, $T=0$ ($T=1$) for isoscalar (isovector) contributions, and by an index K having the values L and T for PC scattering and L,T,T' for PV scattering [here we use tildes to indicate the PV responses and suppress the labels AV and VA in Eq. (8)]. For an isoscalar target like the deuteron, the total response of each type is the sum of $T=0$ and $T=1$ contributions. $\bar{E}=\sqrt{M^2+\mathbf{p}^2}$ denotes the energy that the struck nucleon, whose momentum is $\mathbf{p}$, would have if it were on shell. Following de Forest [12], we also define $\bar{\omega}=E'-\bar{E}$, where $E'=\sqrt{M^2+\mathbf{p}'^2}$ is the energy and $\mathbf{p}'=\mathbf{q}+\mathbf{p}$ is the momentum of the detected (on-shell) nucleon, and use the notation $\bar{Q}^2=\bar{\omega}^2-q^2$ and $\bar{\tau}=|\bar{Q}^2|/4M^2$. The momentum distribution $\rho(p)$ is given by

$$\rho(p)=\int_0^\infty dE\, S(p,E)=\frac{1}{2\pi^2}[u^2(p)+w^2(p)]\ , \tag{25a}$$

where

$$u(p)=\int_0^\infty dr\, rj_0(pr)u(r)\ , \tag{25b}$$

$$w(p)=\int_0^\infty dr\, rj_2(pr)w(r)\ . \tag{25c}$$

Here $S(p,E)$ is the deuteron spectral function and $u(r)$, $w(r)$ are, respectively, the $^3S_1$ and $^3D_1$ ground-state radial wave functions of the deuteron [with $u(p)$ and $w(p)$ the corresponding Bessel transforms given in Eqs. (25b) and (25c)]. The momentum distribution normalization condition is

$$\int_0^\infty dp\, p^2\rho(p)=\frac{1}{4\pi}\ . \tag{26}$$

For the off-shell, single-nucleon responses, $W^K(T=0,1)$ and $\tilde{W}^K(T=0,1)$, we employ generalizations of the cc1 off-shell recipe introduced by de Forest [12] and specialized for use in inclusive scattering [19]:

$$W^L(T=0,1)=\left[\frac{\bar{E}+E'}{2M}\right]^2(G_2^{(T)}+\Delta G^{(T)})-\left[\frac{q^2}{|Q^2|}\right]G_1^{(T)}\ , \tag{27a}$$

$$W^T(T=0,1)=\left[\frac{|\bar{Q}^2|}{q^2}\left[\frac{\bar{E}+E'}{2M}\right]^2-(1+\bar{\tau})\right](G_2^{(T)}+\Delta G^{(T)})+2\frac{\bar{\tau}}{\tau}G_1^{(T)}\ , \tag{27b}$$

$$\tilde{W}^L(T=0,1)=\left[\frac{\bar{E}+E'}{2M}\right]^2[\tilde{G}_2^{(T)}+\Delta\tilde{G}^{(T)}]-\left[\frac{q^2}{|Q^2|}\right]\tilde{G}_1^{(T)}\ , \tag{27c}$$

$$\tilde{W}^T(T=0,1)=\left[\frac{|\bar{Q}^2|}{q^2}\left[\frac{\bar{E}+E'}{2M}\right]^2-(1+\bar{\tau})\right](\tilde{G}_2^{(T)}+\Delta\tilde{G}^{(T)})+2\frac{\bar{\tau}}{\tau}\tilde{G}_1^{(T)}\ , \tag{27d}$$

$$\tilde{W}^{T'}(T=0,1)=2\frac{\bar{\tau}}{q}(\bar{E}+E')G_M^{(T)}\tilde{G}_A^{(T)}\ . \tag{27e}$$

The functions here involving G's are combinations of the Sachs form factors introduced in Eqs. (17):

$$G_1^{(T)}=\tau G_M^{(T)2},\quad \tilde{G}_1^{(T)}=\tau G_M^{(T)}\tilde{G}_M^{(T)}\ ,$$

$$G_2^{(T)}=\frac{G_E^{(T)2}+\tau G_M^{(T)2}}{1+\tau},\quad \tilde{G}_2^{(T)}=\frac{G_E^{(T)}\tilde{G}_E^{(T)}+\tau G_M^{(T)}\tilde{G}_M^{(T)}}{1+\tau}\ ,$$

$$\Delta G^{(T)}=\frac{(\bar{\tau}-\tau)}{(1+\tau)^2}(G_E^{(T)}-G_M^{(T)})^2,\quad \Delta\tilde{G}^{(T)}=\frac{(\bar{\tau}-\tau)}{(1+\tau)^2}(G_E^{(T)}-G_M^{(T)})(\tilde{G}_E^{(T)}-\tilde{G}_M^{(T)})\ , \tag{28}$$

where $T=0,1$. One can check that in the case of a single stationary (on-shell) nucleon these expressions reduce to the one given in Ref. [4] or in Eq. (19) when $Z=1$ and $N=0$. Note that all of the strangeness form factors are isoscalar [see Eqs. (17)]; furthermore, in the standard model at tree level, the entire isoscalar axial-vector contribution comes from $G_A^{(s)}$.

4. *Plane-wave Born approximation (PWBA)*

Other than the difference arising from including the fully relativistic current in PWIA versus expanding to order $(q/M)^2$ as in PWBA, a crucial distinction between the two approximations arises from the fact that only the direct scattering process is taken into account in PWIA;

on the other hand, PWBA (along with the full calculation which includes FSI) also incorporates the exchange process where interferences occur between the amplitudes shown schematically in Fig. 2 (see the discussion above). In the present subsection we discuss the nature of these direct/exchange effects using a simplified PWBA model which has only a $^3S_1$ contribution for the deuteron ground state and which takes into account only the nonrelativistic, on-shell reduction of the cross sections. Our purpose here is to gain a better understanding for the role that the interference contributions play in the PV asymmetry as q and ω are varied. Of course, in presenting most results in the next section, we include both $^3S_1$ and $^3D_1$ components in the deuteron ground state and expand the electroweak operators to order $(q/M)^2$, as discussed above. By comparing the PWIA and the PWBA results we shall be able to establish the kinematic regions where the former becomes a reliable approximation, i.e., where the exchange effects become negligible. This will have important consequences, since then we can employ the PWIA which is presumed to incorporate relativistic aspects of the electroweak single-nucleon currents better than the nonrelativistic expansions, especially at high-momentum transfers.

In this simplified PWBA model we find that the EM response functions have the following dependences:

$$\begin{aligned} R^L(T=0) &\sim G_E^{(0)2}(\mathcal{D}+\mathcal{E}) , \\ R^L(T=1) &\sim G_E^{(1)2}(\mathcal{D}-\mathcal{E}) , \\ R^T(T=0) &\sim G_M^{(0)2}(\mathcal{D}+\mathcal{E}/3) , \\ R^T(T=1) &\sim G_M^{(1)2}(\mathcal{D}-\mathcal{E}/3) , \end{aligned} \tag{29}$$

where

$$\begin{aligned} \mathcal{D} &\equiv \int_{|y|}^{Y} dp\, p\, u^2(p) , \\ \mathcal{E} &\equiv \int_{|y|}^{Y} dp\, p\, u(p)u(p') , \end{aligned} \tag{30}$$

where p' is related to p through $\sqrt{M^2+p^2}+\sqrt{M^2+p'^2}=M_D+\omega$, with similar expressions for the PV responses. As in the PWIA at high q and small $|y|$ it is safe to take $Y\to\infty$. The $\mathcal{D}$ terms correspond to the nonrelativistic, on-shell, $^3S_1$-state-only version of the PWIA, *viz.*, using $\rho(p)=(1/2\pi^2)u^2(p)$. The ratio $\mathcal{E}/\mathcal{D}$, which sets the naive scale for the relative importance of the exchange terms, is shown in Fig. 3 for kinematics corresponding to the impulse approximation position of the QE peak,

$$\omega_{\text{peak}}=\sqrt{M^2+q^2}+\epsilon_D-M , \tag{31}$$

where $\epsilon_D=2M-M_D$ is the deuteron binding energy. The characteristic momentum where this ratio becomes $\frac{1}{2}$ is about 110 MeV/$c\sim 2p_F$, where $p_F\sim 55$ MeV/c is the effective Fermi momentum in the deuteron. We see that the ratio drops dramatically with increasing momentum transfer and thus we should expect that the exchange contributions become unimportant beyond, say, 400–500 MeV/c and accordingly that the PWIA will become justified at sufficiently high q. These expectations are borne out in detail when we examine the results presented in the next section.

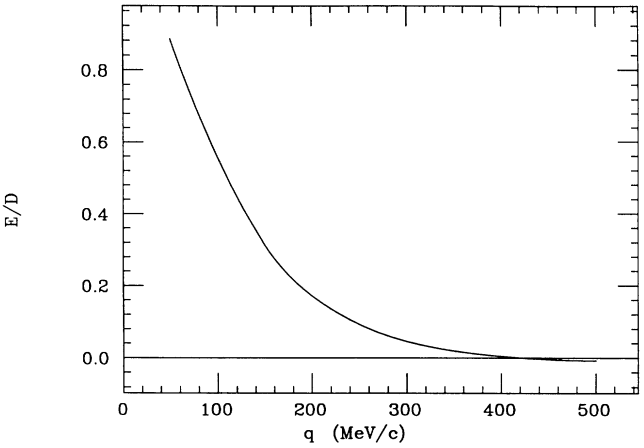

FIG. 3. The ratio of $(\mathcal{E}/\mathcal{D})$ as a function of three-momentum transfer q on the quasielastic ridge, i.e., for $\omega=\omega_{\text{peak}}$ given by Eq. (31). These are results in PWBA with an S-state deuteron.

To see why this happens, let us recall that the y-scaling variable (see, for example, Ref. [19]) is obtained as a solution to the equation

$$M_D+\omega=\bar{E}+E'=\sqrt{M^2+(q+y)^2}+\sqrt{M^2+y^2} . \tag{32}$$

Examining the direct term [$\mathcal{D}$ in Eqs. (30)] we see that the integral has its maximum when $y=0$ and thus $\omega=\omega_{\text{peak}}$, namely, at the QE peak. For fixed $y=0$ the answer is independent of q, since the only other q dependence in this simplified model is contained in Y and becomes negligible when q and $Y\to\infty$. On the other hand, the exchange term [$\mathcal{E}$ in Eqs. (30)] involves an overlap between $u(p)$ and $u(p')$. At $y=0$ we have $\bar{E}+E'=\sqrt{M^2+q^2}+M$, and therefore, as q becomes large so does the sum of $\bar{E}=\sqrt{p^2+M^2}$ and $E'=\sqrt{p'^2+M^2}$. Hence, not both of p and p' can be small at the same time. Since the function $u(p)$ is localized to very small values of p (i.e., most of the momentum distribution lies at $p<p_F\sim 55$ MeV/c), this immediately implies that the ratio $\mathcal{E}/\mathcal{D}$ must fall with increasing q. Similar conclusions do not hold in general for kinematics away from the QE peak. For example, at threshold we have $y=-q/2$ and consequently the lowest allowable values of the momenta in Eqs. (30) are $p_{\min}=p'_{\min}=q/2$. Since at all but the lowest values of q the maximum in both of the integrands in Eqs. (30) will occur when p and p' are at their smallest values [where $u(p)$ and $u(p')$ are maximized], we then deduce that the ratio $\mathcal{E}/\mathcal{D}\to 1$ at threshold; under these conditions, the PWBA and PWIA results can be quite different. In future work we shall return to examine non-QE kinematics in more detail. In the present context, we reiterate the basic result here: at sufficiently high values of q the $(\mathcal{E}/\mathcal{D})$ interference effects should in general diminish and the relativistic PWIA should become applicable.

However, some caution should be exercised even when studying only the region near the QE peak, since the

significance of the ratio $\mathcal{E}/\mathcal{D}$ may be quite different for the various response functions and, ultimately, for the parity-conserving cross section and parity-violating asymmetry, depending on the choice of kinematics. Consider first the longitudinal EM response: for small momentum transfers, $G_E^{(0)} \simeq G_E^{(1)}$, since G_{En} is very small, and therefore $R^L(T=0)+R^L(T=1)$ is basically the same whether the PWBA or PWIA is used [see Eqs. (29)]. When G_{En} becomes appreciable, $\mathcal{E}/\mathcal{D}$ has already dropped dramatically, and thus the conclusion still holds. On the other hand, a different argument is found for the transverse EM terms, where $G_M^{(0)}$ and $G_M^{(1)}$ are rather different (equivalently, G_{Mp} and G_{Mn} are both large and different). As we can see from Eqs. (29), there the scale is given by $\mathcal{E}/3\mathcal{D}$, which suppresses the exchange effects, and hence we see that the PWBA and PWIA results should not be much different as long as $\mathcal{E}/\mathcal{D}$ is not too large. Similar conclusions hold for the transverse PV responses which are also spin-flip dominated. On the other hand, the results obtained for $\tilde{R}^L$ and accordingly for the asymmetry at forward angles can be quite sensitive to $\mathcal{E}/\mathcal{D}$ effects. The reason is that the inclusion of the weak neutral current couplings $\beta_V^{(T=0,1)}$ changes the scale from $\mathcal{E}/\mathcal{D}$, occurring in longitudinal EM studies, to

$$\left[\frac{\beta_V^{(0)}-\beta_V^{(1)}}{\beta_V^{(0)}+\beta_V^{(1)}}\right]\frac{\mathcal{E}}{\mathcal{D}} , \tag{33}$$

which is about $-11\mathcal{E}/\mathcal{D}$ in the standard model (see Sec. II B). For this reason, the parity-violating longitudinal response can be extremely different in the PWIA and PWBA, even leading to opposite signs for the asymmetry obtained near threshold using the two models, as discussed in the next section.

III. RESULTS

In this section we present results using the models discussed in the previous sections. For the single-nucleon form factors we use the parametrizations of Refs. [6–8], including the Galster [21] form for G_{En}. Alternative parametrizations for the electromagnetic form factors [22] were also explored, although no significant differences between the results obtained with the two sets were found; our expectation is that more information will be available to help in minimizing uncertainties from electromagnetic form factors in the near future from work at medium-energy facilities (MIT–Bates, Mainz, NIKHEF) and in the longer term from higher-energy facilities (CEBAF). Less is known about the isovector axial-vector form factor of the nucleon and for that we use the parametrization of Refs. [6–8]. One of our goals is to investigate whether PV QE scattering can serve as a means to determine the neutral current version of this form factor. In Sec. III A, where the nuclear model dependences are discussed, we take all strangeness form factors to be zero and then return in Sec. III B to study what happens when $\bar{s}s$ components are allowed to occur in the nucleon.

We employ two models for the NN interaction which are quite different in their short and medium range behaviors, but are basically phase-shift equivalent, namely, the OBE supersoft core Sprung–de Tourreil model (SdT) [23] and an old-fashion semiphenomenological hard-core Yale model (Y) [24]. These represent extremes in that the former is quite "soft" while the latter is quite "hard." Most state-of-the-art potentials will yield results which fall somewhere between what we find using these extremes. When results are presented for the PWIA and PWBA we use the Bessel transforms of the deuteron ground-state wave functions obtained with the SdT potential.

For a general orientation let us begin by presenting results for the PV asymmetry with specific choices for the kinematics. Following this we return to examine the model dependences in more detail in the next subsection. In Fig. 4 we show the asymmetry at two angles, a typical forward angle (35°) and an extreme backward angle (170°, to emphasize the transverse contributions). The results are shown as functions of ω for a broad range of momentum transfers, $q=150$, 300, 500, 1000, and 1500 MeV/c. In each case the position of the QE peak is indicated by a vertical line. Naturally, in an actual experiment it will be necessary to integrate over some range in energy loss. In fact, the highest statistical precision in a given measurement of the asymmetry will be obtained by maximizing the figure of merit

$$\mathcal{F}=\sigma_{\rm EM}\mathcal{A}^2 , \tag{34}$$

that is, by integrating over the largest region of ω (and solid angle) that is feasible. The QE region, in particular, is the focus of the present work. There we believe that the process is sufficiently "quasifree" to permit the extraction of information about the single-nucleon form factors while minimizing the impact of nuclear model dependences in calculating the asymmetry. This region is defined by the peak position as indicated in Fig. 4 and by the width of the peak, where the latter (full width at half maximum) is given quite well by the relativistic Fermi gas expression [8,20],

$$\Delta\omega=\sqrt{2}qp_F/\sqrt{M^2+q^2} , \tag{35}$$

and results in the values 12, 24, 36, 57, and 66 MeV for $q=150$, 300, 500, 1000, and 1500 MeV/c, respectively, when p_F is taken to be 55 MeV/c. Clearly the QE peak in deuterium is rather well localized and most of the integral will come from contributions close to the peak. If we integrate over the entire QE region, then the figure of merit can be shown (see Ref. [8] where these issues are addressed in more detail) to increase rapidly with q, reaching a maximum in the vicinity of 500 MeV/c, and then slowly to decrease at higher values of momentum transfer. Consequently, the best figure of merit (and so the smallest fractional uncertainty in the asymmetry, $\delta\mathcal{A}/\mathcal{A}$) will occur at intermediate values of q and less precision can be expected at low momentum transfer. From the experimental considerations discussed in Ref. [8] we expect that the PV asymmetry could be determined to about 1–2 % using facilities that will exist in the near future for $q\sim500$ MeV/c, and only to about 5–10 % for $q\sim150$ MeV/c. We shall return shortly to

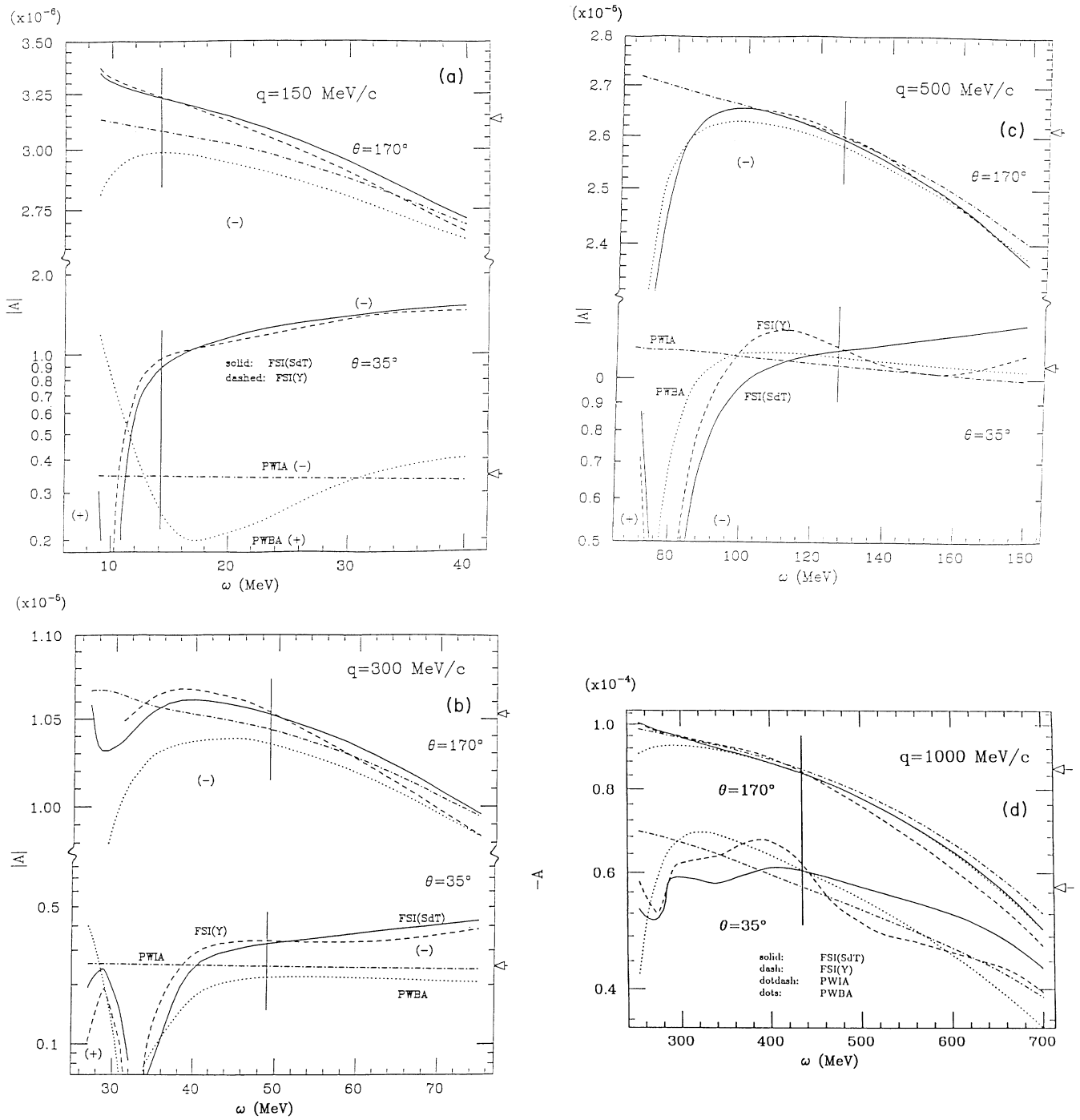

FIG. 4. (a) The magnitude of the parity-violating asymmetry $\mathcal{A}$ as a function of energy transfer ω, at $q=150$ MeV/c for two values of the electron scattering angle θ. The low-ω cutoffs in the curves correspond to inclusive electrodisintegration at threshold. results obtained with different models are shown: FSI with the SdT potential (solid line), FSI with the Yale potential (dashed), PWBA (dots), and PWIA (dot-dashed). The (+) and (−) signs indicate positive and negative values of the asymmetry. The vertical lines indicate the position of the quasielastic peak at $\omega=\omega_{\text{peak}}$ and the arrows at the right-hand edge of the figure indicate the value of $|\mathcal{A}|$ at the QE peak in the static approximation. The width of the QE peak for these kinematics is about 12 MeV. (b) The magnitude of the PV asymmetry $\mathcal{A}$ at $q=300$ MeV/c and $\theta=35°$ and 170°. The lines are as indicated in (a). The width of the QE peak for these kinematics is about 24 MeV. (c) The magnitude of the PV asymmetry $\mathcal{A}$ at $q=500$ MeV/c and $\theta=35°$ and 170°. The lines are as indicated in (a). The width of the QE peak for these kinematics is about 36 MeV. (d) The negative of the PV asymmetry, $-\mathcal{A}$, is shown at $q=1$ GeV/c and $\theta=35°$ and 170°. The lines are as indicated in (a). The width of the QE peak for these kinematics is about 57 MeV. (e) The negative of the PV asymmetry, $-\mathcal{A}$, is shown at $q=1.5$ GeV/c and $\theta=35°$ and 170°. The lines are as indicated in (a), except that only the FSI(SdT) results are shown, since they are indistinguishable from the FSI(Y) results for both angles, and in the $\theta=170°$ case from the PWBA ones too. The width of the QE peak for these kinematics is about 66 MeV.

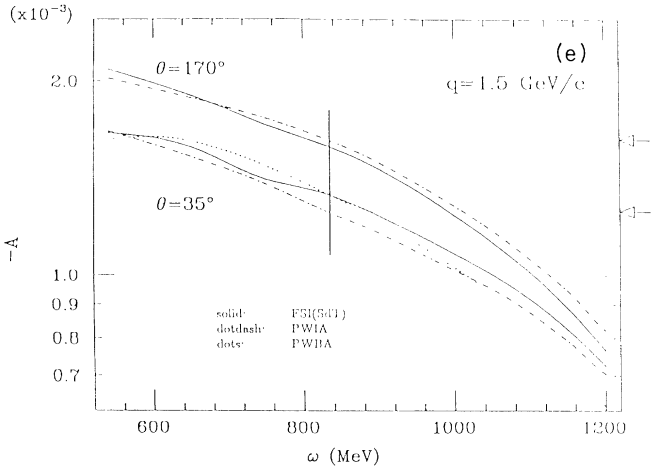

FIG. 4. (*Continued*).

discuss the level of confidence we have in the model results presented here.

Since our focus is on the results in the vicinity of the QE peak, we show the q dependence of the asymmetry in Fig. 5 and the θ dependence for $\omega=\omega_{\text{peak}}$ in Figs. 6. The former displays the general increase of the asymmetry with increasing momentum transfer, principally due to the explicit factor $|Q^2|$ in the asymmetry [see Eq. (7)]. The EM cross section, on the other hand, falls with increasing momentum transfer at constant scattering angle and so yields the characteristic behavior of $\mathcal{F}$ alluded to above. The θ dependence shown in Fig. 6 indicates why measurements at both forward and backward angles are important. Here the asymmetry is written in the form

$$\mathcal{A}=\mathcal{A}_L+\mathcal{A}_T+\mathcal{A}_{T'}\ , \tag{36}$$

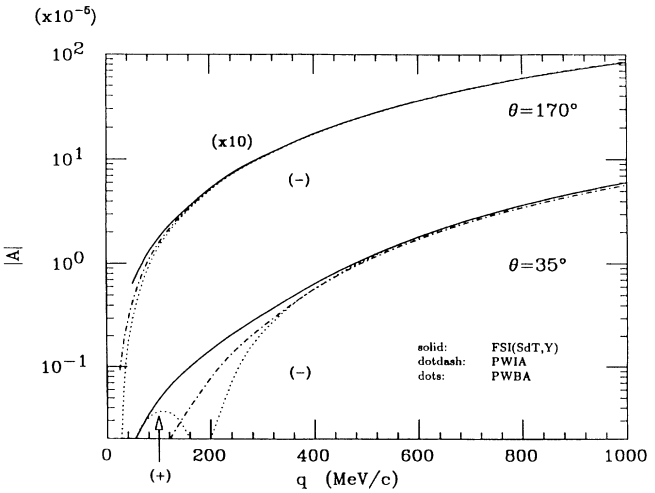

FIG. 5. The magnitude of the asymmetry $\mathcal{A}$ as a function of three-momentum trasnfer q on the quasielastic ridge ($\omega=\omega_{\text{peak}}$) for two electron scattering angles. These results are obtained with different models: FSI(SdT) (solid line), PWBA (dots), and PWIA (dot-dashed).

where the three terms correspond to the three contributions in Eq. (8). The figure shows the ratios $\mathcal{A}_L/\mathcal{A}$ and $\mathcal{A}_{T'}/\mathcal{A}$; clearly the former is emphasized in the forward direction and the latter in the backward direction. For instance, when we are interested in effects which stem from the axial-vector currents, we must choose θ to be large enough to bring out the T' contribution. Under these conditions at $q\sim 500$ MeV/c, for example, the axial-vector term contributes about 18% to the total asymmetry. If the latter could be measured to 1%, then this term would be known to about 5% and, consequently, would yield interesting information about the nucleon's axial-vector form factor. For comparison, at $q\sim 150$ MeV/c the fractional effect of the T' is larger ($\sim 37\%$ at backward angles in Fig. 6), however, since it may be difficult to determine $\mathcal{A}$ to better than $\sim 5-10\%$ (see above), this would only constitute a 14–27% measurement of the axial-vector currents, which is less interesting. Such considerations lead us to favor intermediate values of q. Similar arguments hold for the longitudinal term, $\mathcal{A}_L$. Note that this contribution changes sign in going between $q=150$ and 500 MeV/c. At intermediate-to-high values of momentum transfer $\mathcal{A}_L$ is typically only about 10% of the total asymmetry, and therefore rather high precision is called for if new information is to be forthcoming. As discussed in Ref. [8], the PV longitudinal response is suppressed for two different reasons: either (1) an explicit factor $1-4\sin^2\theta_W\approx 0.092$ occurs multiplying the usual "unsuppressed" form factor G_{Ep}, or (2) a "suppressed" form factor such as G_{En} enters. An exception to these observations might occur, however: namely, the strangeness form factor $G_E^{(s)}$ may not be small at large momentum transfer, as it must at low $|Q^2|$, since it must vanish at $Q^2=0$. In this circumstance, measurements at sufficiently high-momentum transfer might help in shedding light on such strangeness contributions, as discussed in more detail in Sec. III B. At low q the fraction of the asymmetry coming from R_{AV}^L can be quite large [$\sim 70\%$ in Fig. 6(b)], and, consequently, if $\mathcal{A}$ could be determined to the level of about 5–10% discussed above for low-momentum transfer, then $\mathcal{A}_L$ would be known to about 7–14%. As we shall see in Sec. III B, this is not small enough to permit especially sensitive determinations of the nucleon form factor content to be attempted and once again we are led to higher values of q if this is to be the reason for studying QE PV scattering from deuterium.

A. Nuclear model dependences

Having discussed the general features of the QE PV asymmetry, we now present an evaluation of the model dependences found when the various approximations are employed. The first observation is that above some characteristic momentum transfer the model dependence is rather weak. Referring again to Fig. 5, we see that at the QE peak for q beyond about 200 MeV/c the curves for $\theta=170°$ have all coalesced at the level of a few percent into a common asymmetry. We shall return to examine the precise level of agreement more carefully in the

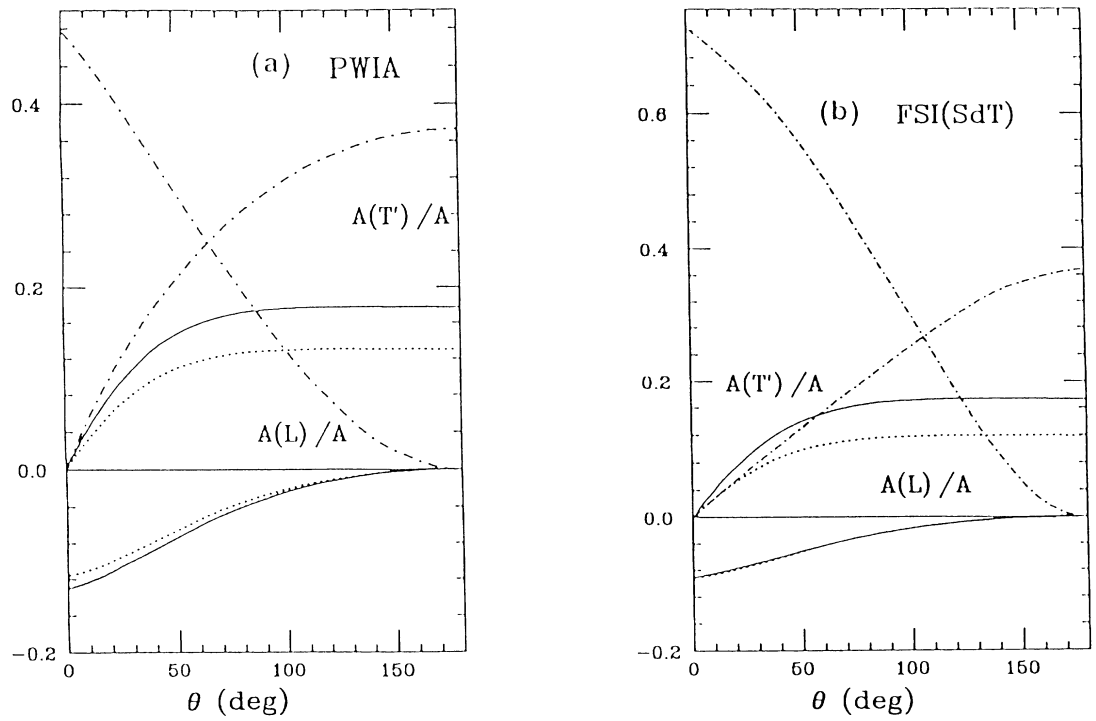

FIG. 6. (a) The relative strength of the PWIA longitudinal (vector) and transverse (axial-vector) current contributions, $\mathcal{A}_L/\mathcal{A}$ and $\mathcal{A}_{T'}/\mathcal{A}$, respectively [see Eqs. (8), (10), and (36)], vs the electron scattering angle θ at $\omega=\omega_{\text{peak}}$. The three lines show results for $q=150$ MeV/c (dot-dashed), 500 MeV/c (solid line), and 1 GeV/c (dots). Note that the $\mathcal{A}_L/\mathcal{A}$ results go to zero at $\theta=180°$ and that the $\mathcal{A}_{T'}/\mathcal{A}$ results go to zero as θ approaches 0°. (b) Same as in (a), but these results are with the FSI(SdT) model. Note the difference in scale between (a) and (b).

discussion a little later. For $\theta=35°$ the degree of convergence is somewhat slower and only beyond about $q=400$ MeV/c do the results fall within the narrow band. We conclude from this that the FSI results should be employed at low-to-medium momentum transfers when high precision predictions are required, for only then is the *np* final state adequately modeled and, especially in the forward direction, the plane-wave approximations will lead to significant errors in the calculated asymmetry. For large scattering angles the latter are somewhat more reliable, reflecting the fact that the dominant currents involve matrix elements of $\sigma\tau$, the spin-isospin-flip operator, which become common factors in the ratio that constitutes the asymmetry and so essentially cancel, producing results which are in better agreement with those using FSI.

Continuing with the behavior on the QE peak, in Fig. 4 we again see significant model dependences at low-momentum transfers which largely disappear at sufficiently high q. In fact, even the static approximation (indicated by arrows at the right-hand edges of the figures) is reasonably successfully at intermediate-to-high values of q, as long as only the peak values of the asymmetry (i.e., where the vertical lines occur in the figures) are compared.

However, when predictions are examined away from the QE peak, the model differences become more apparent. In particular, for values of ω below the peak the models can yield dramatically different results for the asymmetry, even the opposite sign in extreme situations such as for $\theta=35°$ at all but the highest q. For instance, looking at the results for $q=500$ MeV/c [Fig. 4(c)], we see that the asymmetry for $\theta=170°$ is quite similar in all models for ω above about 100 MeV/c (which includes most of the QE response region), but shows considerable model dependence as one approaches threshold. While the spread of the results is somewhat greater for $\theta=35°$ at $q=500$ MeV/c, the qualitative behavior is basically the same. The PWIA results at low ω deviate from those of the FSI and PWBA models, which yield similar results, indicating that the direct/exchange interference effects are playing an important role, whereas the distorting effect of the FSI is not the dominant effect. For higher values of q this threshold behavior goes away [see Fig. 4(e)] and all models, except for the static approximation, yield similar results over a wide range of energies. At lower values of q the near-threshold region is especially model dependent, a fact which is not unexpected, since only a few partial wave are important under these circumstances and the process is no longer "quasifree." The distorting effect of the FSI and the enforcement of orthogonality between initial and final-state wave functions which occurs when they are proper solutions of the Schrödinger equation with a given *NN* potential may lead to rather different asymmetries in the FSI cases than in the PWBA or PWIA cases. In particular, for $\theta=170°$ at

$q=150$ and 300 MeV/c we see the prominent peaking which occurs as threshold is approached that is due to the (transverse, spin-flip) ${}^3S_1+{}^3D_1\rightarrow{}^1S_0$ transition (see also Ref. [25]). Such effects are, of course, only included in the FSI model. As q increases, more partial waves play a role and the relative importance of such strong FSI effects diminishes, so that the process becomes more "quasifree." At $\theta=35°$ and low q results in the different models can be dramatically different, to the extent that at $q=150$ MeV/c the PWBA has the wrong sign, very likely reflecting the lack of orthogonality in that approximation. Curiously, the PWIA does somewhat better.

As discussed above, to extract new information about the single-nucleon form factors which enter into the PV asymmetry we will require fractional precision in the measurements of about $\delta\mathcal{A}/\mathcal{A}\sim 1-2\%$. Consequently, we must look even more carefully into the model dependences in the problem, for, if they are not also rather small, then there will be little hope of understanding the experiments, no matter how well they are performed. In Fig. 7 we show various ratios of asymmetries on expanded scales to show more clearly the nature of the model dependences. Since the reaction is most "quasifree" on the QE peak, and therefore has the least model dependence for values of ω in the vicinity of the peak, we have limited our attention to that region in the figures. Specifically, the ratios of the FSI asymmetry to the PWBA or PWIA asymmetries is displayed. We see that at backward angles for q above about 400 MeV/c these ratios lie within 1% of unity and only deviate from one at lower q (where clearly the FSI model must be employed for high precision predictions). At forward angles the behavior is somewhat different: there the FSI/PWBA ratio drops to unity with increasing q, indicating that the plane-wave approximation is rather good for high enough momentum transfers. However, the FSI/PWIA ratio stays above about 1.05 and so requires some understanding before a choice can be made about which model to believe in a given kinematic region (see below).

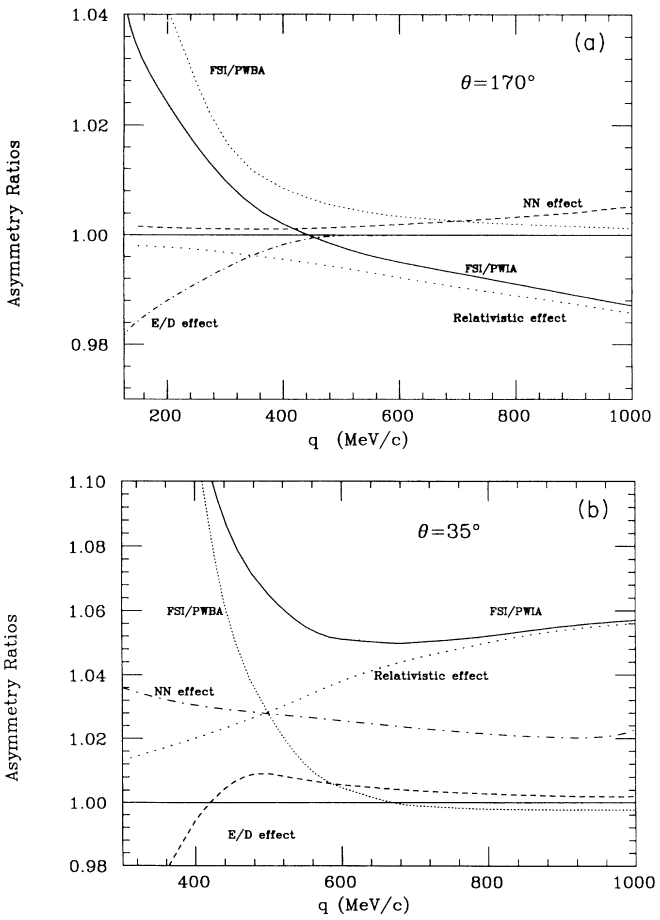

FIG. 7. (a) The sensitivity of the PV asymmetry to various effects is illustrated in the form of asymmetry ratios as a function of three-momentum trasnsfer q, at $\omega=\omega_{\rm peak}$ and $\theta=170°$. The lines marked "NN effect," "E/D effect," and "relativistic effect" are explained in the text. The FSI results are for the SdT model, except for the curve marked "NN effect." (b) Same as in (a), but at $\theta=35°$.

Let us examine several of the model dependences one at a time to aid in choosing which model to employ. We begin with the curves marked "NN effect" in Fig. 7 which show the ratio of the asymmetry obtained with the Yale potential to that obtained with the Sprung–de Tourreil potential. For the 170° case we see that this ratio is within about 1% of unity for $q>400$ MeV/c, while for 35° it is a little larger, dropping to about 2% from unity at high q. To the extent that these potentials provide extremes in modeling the NN interaction, we should expect that the NN model dependence is actually less than this and so satisfies the criterion of 1–2% model uncertainty, as long as the momentum transfer is kept above, say, 400–500 MeV/c. At low q, however, the NN model dependence is larger; we may ultimately be able to turn the problem around in that kinematic region and learn something about the potentials themselves.

The curves marked "E/D effect" in Fig. 7 show what happens when we form the ratio of the PWBA asymmetry with the exchange terms set to zero over the complete PWBA asymmetry (i.e., with both direct and exchange terms present). The former is the derelativized, on-shell PWIA (see Sec. II C 4), and so this ratio serves to tell us where the interference effects become unimportant. At $\theta=170°$ we see deviations from unity at the 1% level only below $q\sim 300$ MeV/c and only below about 400 MeV/c for 35°. Thus we might hope that the PWIA is valid as a model for the PV asymmetry at the 1–2% level as long as the momentum transfer lies above about 400 MeV/c.

The curves marked "Relativistic effect" show the ratio of the asymmetry at the QE peak when the currents are derelativized in the same way as in the FSI and PWBA calculations and used in the PWIA compared with the relativistic PWIA where no expansions in powers of (q/M) are required. This provides a measure of how important the truncation of the currents to terms of $O((q/M)^2)$ is in obtaining the asymmetry. We see that the effect grows with increasing momentum transfer, reaching about 1% (6%) at $q=1$ GeV/c for $\theta=170°$ (35°). The fact that the effect is larger in the forward direction is not unexpected, since we know that there are

important relativistic corrections of order $(q/M)^2$ in the longitudinal responses (Darwin-Foldy and spin-orbit contributions [13]). We observe that the source of the differences between the FSI and PWIA approaches at high q is entirely this relativistic effect; in particular, we can see from the results presented in Fig. 7 (in the curves labeled "E/D effect" and "FSI/PWBA") that neither the exchange terms nor the distorting effect of the NN interaction in the final state are important at high q. Since only the PWIA contains terms of all orders in (q/M), we are thus led to expect that the latter model has more validity at high-momentum transfers (say, above roughly 500 MeV/c).

From all of these considerations of the PV asymmetry at the QE peak we see that for backward scattering angles the FSI model should be employed for q below about 400 MeV/c and that the PWIA can be used for momentum transfers above this value. Very little error would be incurred, however, if the FSI model were to be used for the entire range of momentum transfer studied at large scattering angles. On the other hand, the forward-angle regime is somewhat different. Again, at low q the FSI model must be employed. Specifically, the relativistic effects fall below 1% if q is less than about 300 MeV/c and so the FSI model should be adequate. For q above about 500 MeV/c the FSI/PWBA ratio and the $\mathcal{E}/\mathcal{D}$ effect both fall to within about 1% of unity and so the PWIA can be used reliably for this value of momentum transfer or higher, as it must, since the relativistic effects become increasingly important there. In between ($q \sim 300-550$ MeV/c) there is no model which can be used with confidence at the 1% level, although from Fig. 7(b) it is not unreasonable that the uncertainty lies perhaps at or below the 3% level.

In actual experiments energy integrations over some region in the vicinity of the QE peak will likely have to be performed to obtain the high statistical precision required. As discussed above the width of the QE response region is quite small, since the deuteron is so weakly bound and hence has a very small effective Fermi momentum. The situation in Fig. 4(c) is typical: there the width of the QE response is only about 36 MeV and consequently most of the results (as measured by the figure of merit, see above) comes from energies between about 109 and 145 MeV. In that narrow region the NN model dependence is quite regular. The two FSI curves cross near the QE peak and clearly any symmetrical integration over this limited region will yield model dependences which are about the same as those at the peak alone. In contrast, if any asymmetrical integration is performed, say, by restricting one's attention to the y-scattering region ($y<0, \omega<\omega_{\text{peak}}$), then the model dependences can grow significantly beyond the 1% level.

Another comment is relevant at this point: when the momentum transfer becomes very large, it becomes more difficult to avoid the region of π production. For instance, in Fig. 4(e) the threshold for π production is at about 633 MeV. Since the PV asymmetry now has a different component (which is not treated in the present work), it will require further study before the level of model uncertainty can be quantified. In this case, if one wishes to minimize these effects, then it will be necessary to restrict one's attention to the y-scaling region and accordingly to perform an asymmetric energy integration. Fortunately, as seen in Fig. 4(e), the model dependence even off the QE peak is rather weak.

B. Determination of single-nucleon form factors using PV QE electron scattering

Finally, we discuss the sensitivity found in the PV asymmetry to specific models for the single-nucleon form factors. We take the electromagnetic form factors to be fixed (see Sec. II B) and concentrate on the axial-vector and strangeness form factors. In particular, we wish to highlight the different behavior found in PV elastic scattering from the proton (discussed in detail in Refs. [4,6]) and the present case of QE scattering from deuterium. To obtain a feeling for the general dependences found in these two cases, let us begin with the static approximation in Eq. (19): at large scattering angles where the transverse contributions are dominant the form factors $G_M^{(s)}$ and $G_A^{(s)}$ are multiplied by the combination $ZG_{Mp}+NG_{Mn}$, whereas the isovector axial-vector form factor, $G_A^{(1)}$ is multiplied by the combination $ZG_{Mp}-NG_{Mn}$. Thus the relative weighting of the former two compared to the latter is

$$\frac{ZG_{Mp}+NG_{Mn}}{ZG_{Mp}-NG_{Mn}} = \begin{cases} 1 \text{ for the proton,} \\ \dfrac{\mu_p+\mu_n}{\mu_p-\mu_n} \simeq 0.187 \text{ for the deuteron ,} \end{cases} \tag{37}$$

so that the effects due to $G_M^{(s)}$ and $G_A^{(s)}$ are suppressed in QE scattering (see also Ref. [8]). Furthermore, the strangeness axial-vector contributions are multiplied by a_V instead of a_A, as can be seen in Eq. (19), which further suppress the effect of these terms in the asymmetry. Henceforth, we ignore $G_A^{(s)}$ and focus on the remaining form factors. These simple arguments suggest the following strategy: by studying elastic PV scattering from the proton and QE scattering from the deuteron at backward angles, it should be possible to separate the effects due to $G_M^{(s)}$ from those due to $G_A^{(1)}$, whereas measurements on the proton along cannot yield such a separation.

To obtain quantitative predictions for the different dependences we use the following parametrizations [6–8] for the relevant form factors:

$$\begin{aligned} G_A^{(1)} &= g_A^{(1)}/(1+3.53\tau)^2 , \\ G_M^{(s)} &= \mu_s/(1+4.97\tau)^2 , \\ G_E^{(s)} &= \rho_s\tau/(1+4.97\tau)^2 , \end{aligned} \tag{38}$$

where the last is discussed more below. At the tree level in the standard model we have $g_A^{(1)}=1.26$ from β decay and from current modeling of the $\bar{s}s$ content in the nucleon (see, e.g., Refs. [26,27]) we expect the strangeness parameters to lie in the ranges $-1<\mu_s<0$ and $-3<\rho_s<0$. We then express the PV asymmetry in the following form:

$$\mathcal{A} = \mathcal{A}_1(1+b_A g_A^{(1)} + b_M\mu_s + b_E\rho_s) , \tag{39}$$

where the numbers $(\mathcal{A}_1;b_A,b_M,b_E)$ reflect the way the asymmetry depends on these three particular form factors. From the considerations presented in the first part of this section let us compare the asymmetries obtained in elastic proton scattering and for QE scattering from the deuteron at the peak for a momentum transfer of 500 MeV/c and a scattering angle of 150°, which is typical for a large solid angle detector. The corresponding incident electron energy for these kinematics is $\epsilon_1=321$ MeV. We obtain

$$\begin{aligned}(\mathcal{A}_1;b_A,b_M,b_E)&=(-1.54\times10^{-5};0.197,-0.461,-0.005)\ \text{proton elastic}\\&=(-2.07\times10^{-5};0.166,-0.070,-0.003)\ \text{deuteron QE-FSI(SdT)}\\&=(-2.07\times10^{-5};0.166,-0.068,-0.003)\ \text{deuteron QE-FSI(Y)}\\&=(-2.06\times10^{-5};0.168,-0.073,-0.002)\ \text{deuteron QE-PWIA}\ .\end{aligned}\tag{40}$$

Clearly the effects due to $G_E^{(s)}$ are very small at backward angles, as expected. All of the models for deuterium used here give answers which are very similar and show again the rather weak-model dependence for these (favorable) kinematics. However, the above expectations concerning the differences between the proton and deuteron cases are borne out in detail. Importantly, the relative dependence on the magnetic strangeness form factor (embodied in the parameter μ_s) is more than six times stronger in the proton case than for the deuteron. Clearly the latter case is relatively more sensitive to the isovector axial-vector form factor (represented by the parameter $g_A^{(1)}$). A high enough precision measurement of the QE PV asymmetry in deuterium should help in defining $G_A^{(1)}$ and so, used in concert with elastic PV scattering from the proton, permit $G_M^{(s)}$ to be determined with better precision than is possible with the proton along (see also Ref. [6]).

At forward scattering angles the situation is somewhat different. Referring again to the static approximation in Eq. (19) for guidance, we see that the terms containing the strangeness electric form factor may now play a role. There, $G_E^{(s)}$ is multiplied by the combination $ZG_{Ep}+NG_{En}$ in the general case for this simple model. However, since G_{En} is so small relative to G_{Ep}, the weighting factor is only weakly dependent on the target nucleus. To obtain a quantitative measure of the form factor sensitivities we present results for a specific forward scattering angle, $\theta=12.5°$, which is in fact the smallest possible for the hall A spectrometers at CEBAF. We again intercompare results for elastic scattering from the proton and scattering at the QE peak for deuterium. Two momentum transfers are considered, $q=150$ and 1000 MeV/c (with corresponding incident electron energies $\epsilon_1=693$ and 4362 MeV, respectively). In the former the value of τ is quite small (0.006) and so the electric strangeness effects are rather weak; however, at the high-q value we have $\tau=0.23$ and consequently they can be strong if $G_E^{(s)}$ is not suppressed [recall from Eq. (38) the electric strangeness form factor is proportional to τ at low-momentum transfer]. We obtain the following for the asymmetries at $q=150$ MeV/c:

$$\begin{aligned}(\mathcal{A}_1;b_A,b_M,b_E)&=(-2.29\times10^{-7};0.039,-0.152,-0.053)\ \text{proton elastic}\\&=(-7.84\times10^{-7};0.028,-0.012,-0.011)\ \text{deuteron QE-FSI(SdT)}\\&=(-8.57\times10^{-7};0.026,-0.010,-0.010)\ \text{deuteron QE-FSI(Y)}\ ,\end{aligned}\tag{41}$$

where only the FSI results are given for the deuteron in light of the discussions in the previous subsection. At such a low-momentum transfer the NN model dependence is not negligible (the overall asymmetry coefficient $\mathcal{A}_1$ differs by about 9% for the two FSI models). The effects due to the three form factors under study here only enter at the few percent level and consequently these kinematics are not too favorable for extracting them. The proton case could be used if both $G_A^{(1)}$ and $G_M^{(s)}$ can be determined well enough using backward-angle scattering from both the proton and the deuteron (see above). The $q=1000$ MeV/c results are the following:

$$\begin{aligned}(\mathcal{A}_1;b_A,b_M,b_E)&=(-3.43\times10^{-5};0.035,-0.495,-0.172)\ \text{proton elastic}\\&=(-5.25\times10^{-5};0.028,-0.080,-0.085)\ \text{deuteron QE-FSI(SdT)}\\&=(-5.40\times10^{-5};0.027,-0.073,-0.078)\ \text{deuteron QE-FSI(Y)}\\&=(-4.87\times10^{-5};0.032,-0.082,-0.108)\ \text{deuteron QE-PWIA}\ .\end{aligned}\tag{42}$$

In this case the two FSI models differ in $\mathcal{A}_1$ by less than 3% and yet the relative effect of $G_E^{(s)}$ could be as large as 16–17% in the FSI models (or 22% in the PWIA) if $\rho_s = -2$ as in the model of Ref. [26]. As discussed in the previous subsection most of the difference between the FSI and PWIA results are due to the nonrelativistic expansion procedure used in the former; for the purpose of predicting the asymmetry at high-momentum transfer the PWIA should be more reliable. Comparing the proton and deuteron results, we again see rather striking differences. In elastic scattering from the proton at forward scattering angles the effects from $G_M^{(s)}$ are quite important and any significant uncertainty in this form factor from backward-angle determinations will propagate into connected uncertainty in $G_E^{(s)}$, no matter how precisely the small angle proton asymmetry is measured. However, taken again together with the QE PV asymmetry on the deuteron where the magnetic strangeness dependence is much weaker, it should be possible to refine our knowledge about all of these various contributions.

IV. CONCLUSIONS

In the present work we have studied the behavior of the parity-violating electron scattering asymmetry for the inclusive reaction $^2\mathrm{H}(\vec{e},e')np$ in the region of the quasielastic peak. We have considered a wide range of momentum transfers, $q = 150 - 1500$ MeV/c, and investigated the nature of the PV asymmetry at large and small values of the electron scattering angle θ. Several models for the electromagnetic and weak neutral currents involved in the electrodisintegration of deuterium have been employed in our work and we find that the asymmetry in the vicinity of the QE peak is very stable except at low-momentum transfers (i.e., the model dependences are seen to be rather weak for such "quasifree" kinematics). We conclude that by using two specific models we are able to provide predictions for the asymmetry spanning this wide range of momentum transfers which are uncertain only at the 1–2 % level. Specifically, for q less than about 500 MeV/c, where direct-exchange and FSI effects are important, we find that only a model which treats these aspects of the problem [such as the FSI(SdT) and FSI(Y) models discussed in the present work] should be employed. On the other hand, these effects are seen to be absent at high q; since there relativistic effects become increasingly important, we conclude that only a model such as PWIA which incorporates relativistic effects in the electroweak operators to all orders in $(q/M)^2$ can be taken to high-momentum transfer.

Our modeling has shown uncertainties in the PV asymmetry to be at the 1–2 % level. While such claims would be difficult to accept for the individual response functions, it should be re-emphasized that the asymmetry is a *ratio* of responses and so contains much less sensitivity to the detailed nature of the reaction mechanism involved. For example, at large scattering angles, where the asymmetry is dominated by transverse contributions, it is straightforward to understand why such a ratio should be rather stable: it is made up of response functions in both its numerator and denominator that are driven by essentially the same currents. Specifically they are all proportional to matrix elements of the spin-isospin-flip operator (whether vector or axial vector in character) and these common matrix elements cancel in forming the ratio. Only when isoscalar or relativistic effects (both of which are suppressed) are incorporated do we see any model dependence in the present analysis. Before we can be completely certain about the reliability of the modeling there are a number of issues which should be addressed, specifically, the roles played by meson-exchange currents and isobar configurations, by NN interactions which include parity-violating pieces and by relativistic dynamics. All such effects are thought to be small along the QE ridge for the range of kinematics under study. Some of these issues will be addressed in the future as natural extensions of our current work.

We have focused on the region around the QE peak, for there we expect the models to be most applicable. Of course, any actual experiment will have to integrate over some finite range of energy. To achieve the highest statistics the optimal region might be reasonably broad, spanning perhaps 30–50 MeV or more. Consequently, it is important to have some idea about how the model dependences will behave in non-QE kinematics. Fortunately, since the deuteron has a very small effective Fermi momentum (~ 55 MeV/c), the figure of merit for performing QE PV measurements is sharply peaked in the QE region. Nevertheless, we have presented results for a wide range of energy away from the QE peak: for kinematics below the peak ($y < 0$) and especially near threshold, we may find significant model dependence, notably at low q. Clearly, if the goal is to minimize the nuclear model dependence in order to learn something about the nucleon's form factors, then this region would appear to be less favorable than the QE region. At energies above the QE peak ($y > 0$) a different consideration becomes a factor: there, at high-momentum transfer, pion production may become important in the QE region. If one is to explore the asymmetry in this case, then it will be necessary to provide a model for PV π production, including both nonresonant terms and contributions that proceed through the Δ. In a future work we shall return to examine the PV asymmetry for non-QE kinematics in more detail. In the present context where the focus has been the region near the QE peak, we have found that the theoretical and experimental aspects of the problem are commensurate, *viz.*, both imply that the relevant level of precision in such studies is about 1–2 %.

Given uncertainties as small as these, we have proceeded to explore the possibility of using PV QE scattering from deuterium to learn something about the form factors of the nucleon. We find that measurements at backward angles and momentum transfers around 500 MeV/c appear to be very well suited to determining the isovector axial-vector form factor $G_A^{(1)}$. PV QE scattering is much less sensitive to the magnetic strangeness form factor $G_M^{(2)}$ than is elastic PV scattering from the proton and therefore we conclude that the combination of $^2\mathrm{H}$ QE and $^1\mathrm{H}$ elastic PV studies could permit the separation of the two form factors. In contrast to this, using only the proton

there will continue to be an inseparable uncertainty which stems from $G_A^{(1)}$ incurred in attempting to extract $G_M^{(s)}$, no matter how precisely such a measurement could be undertaken. Finally, at high-momentum transfers, 1 GeV/c or more, our results for forward-angle scattering suggests that the electric strangeness form factor $G_E^{(s)}$ could also be studied by combining PV electron scattering measurements using the deuteron and the proton.

ACKNOWLEDGMENTS

It is a pleasure to thank M. J. Musolf and S. B. Kowalski for useful discussions during the course of this work. This work is supported in part by NSF Grant No. PHY-8911416 and in part by funds provided by the U.S. Department of Energy under Contract No. DE-AC02-76ER03069.

[1] S. Weinberg, Phys. Rev. Lett. **19**, 1264 (1967); A. Salam, in *Elementary Particle Physics,* edited by N. Svartholm (Stockholm, 1968), p. 367; S. L. Glashow, J. Iliopoulos, and L. Maiani, Phys. Rev. D **2**, 1285 (1970).
[2] J. D. Walecka, Nucl. Phys. **A285**, 349 (1977).
[3] T. W. Donnelly and R. D. Peccei, Phys. Rep. **50**, 1 (1979).
[4] T. W. Donnelly, J. Dubach, and I. Sick, Phys. Rev. C **37**, 2320 (1988).
[5] T. W. Donnelly, J. Dubach, and I. Sick, Nucl. Phys. **A503**, 589 (1989).
[6] M. J. Musolf and T. W. Donnelly, Nucl. Phys. A (to be published).
[7] M. J. Musolf, T. W. Donnelly, J. Dubach, E. J. Beise, S. B. Kowalski, and S. J. Pollock (unpublished).
[8] T. W. Donnelly, M. J. Musolf, W. M. Alberico, M. B. Barbaro, A. De Pace, and A. Molinari, Nucl. Phys. A (to be published).
[9] E. Hadjimichael and E. Fishbach, Phys. Rev. D **3**, 755 (1971).
[10] H. Arenhövel, Nucl. Phys. **A384**, 287 (1982).
[11] T. de Forest, Jr., Ann. Phys. (N.Y.) **45**, 365 (1967); C. Cioffi degli Atti, E. Pace, and G. Salmé, Phys. Rev. C **36**, 1208 (1987); M. Bernheim, A. Bussiere, J. Mougey, D. Royer, D. Tarnowski, S. Turck-Chieze, S. Frullani, G. P. Capitani, and E. De Sanctis, Nucl. Phys. **A365**, 349 (1981).
[12] T. de Forest, Jr., Nucl. Phys. **A392**, 232 (1983).
[13] T. de Forest, Jr., and J. D. Walecka, Adv. Phys. **15**, 1 (1966).
[14] T. W. Donnelly and J. D. Walecka, Annu. Rev. Nucl. Sci. **25**, 329 (1975).
[15] J. Ellis and G. L. Fogli, Phys. Lett. B **249**, 543 (1990).
[16] P. Langacker, U. Penn Report No. UPR-0435T, 1990.
[17] G. Altarelli, Nucl. Phys. (Suppl. Proc.) **B19**, 354c (1991).
[18] R. G. Sachs, Phys. Rev. **126**, 2256 (1962).
[19] D. B. Day, J. S. McCarthy, T. W. Donnelly, and I. Sick, Annu. Rev. Nucl. Part. Sci. **40**, 357 (1990).
[20] W. M. Alberico, A. Molinari, T. W. Donnelly, E. L. Kronenberg, and J. W. Van Orden, Phys. Rev. C **38**, 1801 (1988).
[21] S. Galster, Nucl. Phys. **B32**, 221 (1971).
[22] F. Iachello, A. D. Jackson, and A. Landé, Phys. Lett. **43B**, 191 (1973).
[23] R. de Tourreil and D. W. L. Sprung, Nucl. Phys. **A201**, 193 (1973); R. de Tourreil, B. Rouben, and D. W. L. Sprung, *ibid.* **A242**, 445 (1975); J. Coté, B. Rouben, R. de Tourreil, and D. W. L. Sprung, *ibid.* **A273**, 269 (1976).
[24] G. Breit, Rev. Mod. Phys. **39**, 560 (1967); R. E. Seamon, K. A. Friedman, G. Breit, R. D. Haracz, J. M. Holt, and A. Prakash, Phys. Rev. **165**, 1579 (1968).
[25] W-Y. P. Hwang and T. W. Donnelly, Phys. Rev. C **33**, 1381 (1986).
[26] R. L. Jaffe, Phys. Lett. B **229**, 275 (1989).
[27] N. W. Park, J. Schlechter, and H. Weigel, Phys. Rev. D **43**, 869 (1991).